Current-Injection Two-Dimensional Photonic Crystal Slab Microcavity

Undergraduate Honor Thesis by

Pantana Tor-ngern

Department of Electrical and Computer Engineering
Duke University
Durham, North Carolina

(Submitted April 21, 2009)

Acknowledgements

First of all, I would like to thank Dr.Yoshie, my advisor, for all his advices and support throughout the project. He is my great inspiration to pursue my graduate study in nanophotonics. I would also like to acknowledge Dean Absher for giving me the opportunity to discover my interest in research through the Pratt Fellow Program. I would like to pay my gratitude to Lingling Tang, the PhD student in the Duke Nanophotonic Group, for her fruitful discussions, trainings and friendship. Many thanks to the Duke Nanophotonic Group for creating the scientific environment for me to enjoy. Thank you all my friends here at Duke for moral support and motivation. Finally, I would like to dedicate this thesis to my parents. I love both of you very much.

Abstract

Electrically-driven photonic crystal lasers have been recently demonstrated.[8] This breakthrough indicates the feasibility of incorporating ultra-small lasers with semiconductor integrated optical circuit. However, this design requires complicated fabrication procedures and lacks good heat sink. In order to resolve these challenges, we propose a two-dimensional (2D) photonic crystal slab sandwiched by metal in place of the conventional free-standing (air-cladding) structure. We use Indium Tin Oxide (ITO) as the metal in our design since it has relatively low optical absorption. Our simulation results suggest that it is possible to achieve lasing operation despite the absorptive property of ITO. Planar photonic crystal microcavities clad by ITO were analyzed to determine the resonant mode inside photonic band gap (PBG) and the quality (Q) factor using finite-difference time-domain (FDTD) technique. Fabrication process is under investigation

Table of Contents

Chapter 1: Overview

1.1 Motivation

Nanoscale technologies have become one of the most popular areas in research nowadays, particularly the nanophotonic technology. Many research groups all around the world actively study and invent compact photonic devices that will compose a photonic circuit in which light carries information, analogous to the electrons which transmit data in the electrical circuit. Figure 1 shows an example of a photonic circuit that has not been fully invented. The red paths which are, for example, photonic waveguides direct light through the entire circuit. Other structures in the figure can be photonic crystal devices which are of our interest. These functional devices play many roles in the circuit such as generating photons, detecting the output, converting photonic signal to electrical signal to be further integrated with the electrical circuit, etc. The photonic circuit has many advantages. Since nothing can travel faster than light, the data transmission in the photonic crystal is very rapid. The data bandwidth is much larger than that in electronics. In addition, the circuit can be so compact that it may be able to fit the whole "laboratory" to investigate a particular problem, resulting in the technology called lab-on-a-chip.

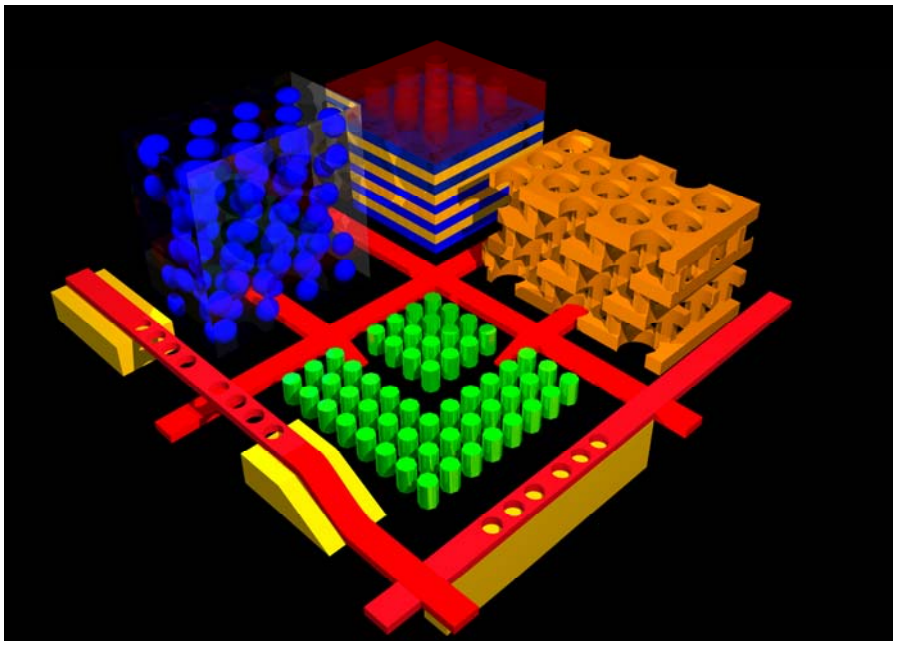

Figure 1: The illustration of a photonic circuit.[4]

This thesis will primarily focus on the investigation of current-injection photonic crystal microlaser. Since most of photonic crystal microlasers are realized by optical pumping, an external laser is needed to excite the photonic crystal resonator. This optically-pumped microcavity is an excellent test bed for the investigation of microcavity physics, but this is impractical for compact optical circuits. Thus, we would like to build the current-injection photonic crystal microlaser. This type of laser utilizes electrical current to induce stimulated emission within the microcavity. To supply the current, we need ohmic metal contacts to the device, thus eliminating the photon source and reducing the space in the circuit.

1.2 The Challenge

In 2004, researchers from the Korea Advanced Institute of Science and Technology demonstrated the first electrically pumped photonic crystal laser[8]. The structure is illustrated in figure 2. The electrical current is injected through the semiconductor post at the center of the structure. Electrons are supplied from the top electrode while the holes are injected directly through the bottom post. The carriers then recombine and generate photons which will excite the photons inside the active region of the photonic crystal, resulting in the stimulated emission. The quality (Q) factor obtained from this structure is approximately greater than 2500. This value degrades rapidly as the post size increases. However, a small post is very difficult to fabricate and leads to mechanical instability, electrical resistance and thermal problems. As a result, we propose a simpler design for the current-injection photonic crystal laser which would resolve the electrical resistance problems and the difficulty in fabrication.

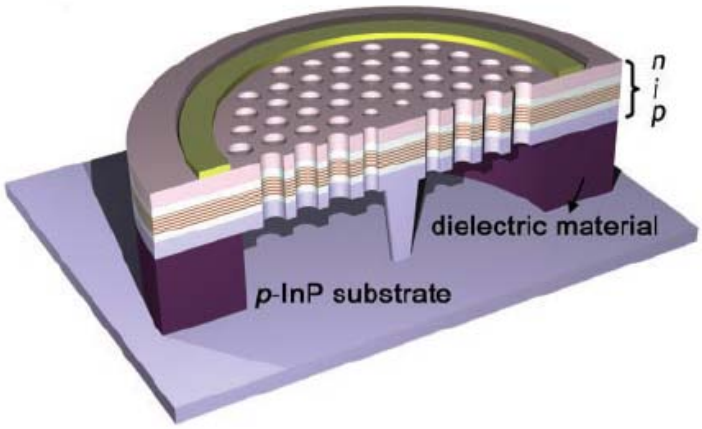

Figure 2: Schematic diagram of the first current-injection photonic crystal laser.[8]

Chapter 2: Background

2.1 Two-dimensional Photonic Crystal

In the world of electronic materials, a crystal lattice occurs when a fundamental building block of atoms or molecules is repeated in space. As a result, a crystal provides a periodic potential to an electron propagating through it. The geometry of the crystal governs its conduction properties. In particular, the lattice may introduce gaps into the energy band structure of the crystal which forbids electrons to travel in certain directions. In the optical regime, a photonic crystal plays the same role as the electronic crystal. The periodic potential in the photonic crystal is originated from a lattice of dielectric media instead of atoms. The difference in dielectric constants of the materials in the crystal creates the similar phenomena for light waves as the atomic potential does for electron waves. Thus, we can manipulate light propagation by designing and constructing photonic crystals with photonic band gaps to prevent light from traveling in certain directions with some specified energies.

The confinement of light can be imposed in three dimensions resulting in three different types of photonic crystal structures. However, this thesis will focus on the two dimensional (2D) slab structure whose periodicity is present in two directions only. Although three dimensional (3D) photonic crystals seem to be the best candidate to completely mold light propagation in all directions, the 2D photonic crystal slab platform is the most popular structure that most photonic devices are based on because its fabrication process is easier than that of the 3D one. To allow the light confinement in the third direction in a 2D photonic crystal, we utilize the concept of total internal reflection (TIR) at the interface of the photonic crystal slab and the cladding material or the environment surrounding the slab. Therefore, a two-dimensional photonic crystal consists of a semiconductor slab perforated with a lattice of holes in two dimensions. The refractive index of these holes is different from that of the slab. The slab is surrounded with a low-index material which is usually air so that light is confined in the slab. In such structure, light is confined by Bragg diffraction through the lattice in lateral direction and by TIR in the vertical direction.

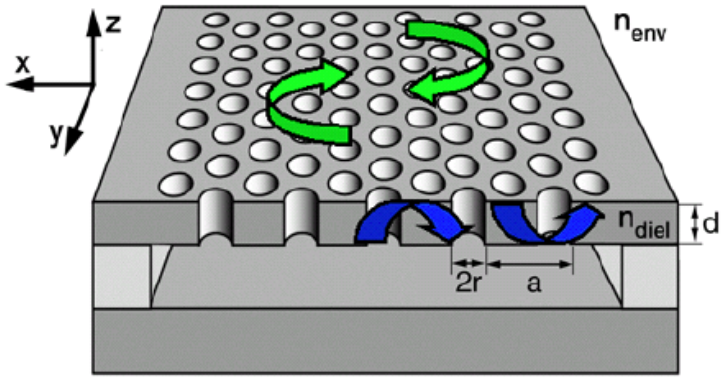

Figure 3: 2D photonic crystal slab: Green arrows show the confinement resulted from the lattice in the slab and the blue arrows represent the vertical confinement by TIR.[7]

Notice that for the 2D photonic crystal as shown in figure 3, the third dimension or the vertical direction is not periodic. Consequently, only light waves with some incident angles at the interface between the slab and the cladding are confined within the slab. This critical angle is given by

$$\theta_c = \sin^{-1}\left(\frac{n_2}{n_1}\right) \tag{1}$$

where θ_c is the incident angle at the interface (critical angle), n_1 is the refractive index of the dielectric slab and n_2 is the refractive index of the cladding material.

Light waves whose incident angles are larger than the critical angles are reflected back and forth inside the slab whereas those with smaller incident angles can escape from the slab. The escaping photons represent energy leaking from the slab, indicating the loss mechanism of the 2D photonic crystal. Hence, we need to take into account the vertical loss when designing and fabricating the photonic crystals. Accordingly, we introduce the concept of light line in the analysis of 2D photonic crystal, specifically in the band diagram calculation. The light line is used to distinguish the radiative modes or leaky modes from the guided modes within the slab. Figure 2 illustrates an example of the band diagram. The region between the green and blue lines is the photonic band gap which prohibits light propagation. The solid line denotes the light line and the grey region represents the radiative modes. Here, the incomplete band gap in 2D photonic crystal is emphasized since the radiative modes exist at all frequencies including the gap. However, complete band gap still exists for the guided modes which are the lines under the light cone. Thus, the ultimate goal of designing a 2D photonic crystal laser is to calculate the photonic band diagram and find the photonic band gap in the material of interest.

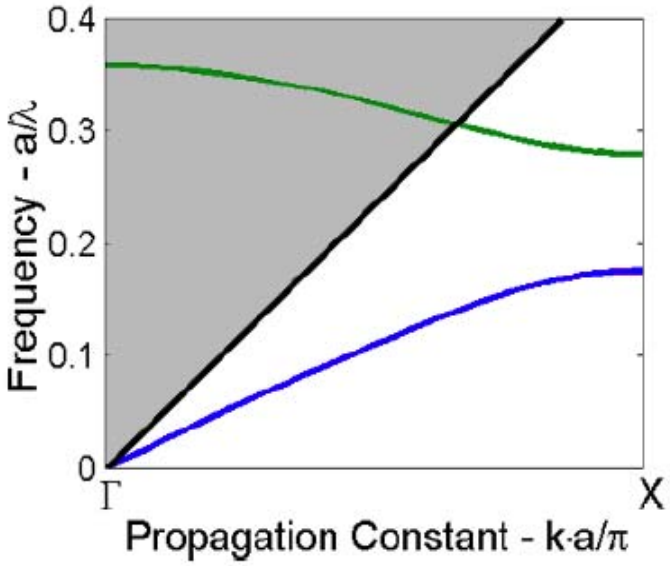

Figure 4: A dispersion diagram of the square lattice 2D photonic crystal along the ΓX direction.[7]

As an example of a band diagram calculation, we consider a triangular photonic crystal lattice as in figure 5. In [7], the analysis of band diagram for the triangular structure patterned on a silicon slab suspended in the air is discussed. The band diagram is obtained by using the 3D finite-difference time-domain (FDTD) technique as illustrated in figure 6 with 20 computational

points per lattice constant (a = 20). The silicon slab thickness is d = 0.55a and hole radius is r = 0.4a. The refractive index of silicon is assumed to be 3.5.

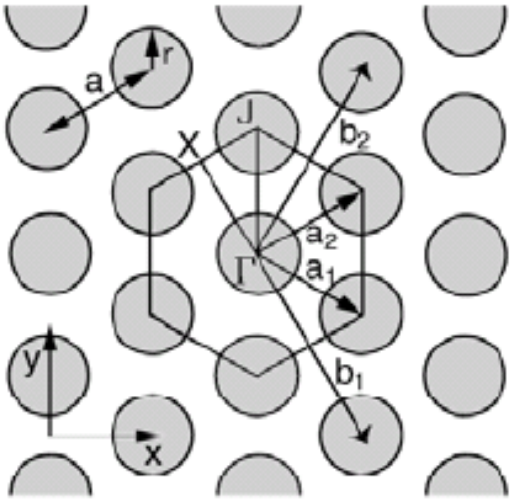

Figure 5: Triangular lattice. Hexagon is the first Brillouin zone with high symmetry points indicated as X J and Γ. The parameters a is the lattice constant and b is the reciprocal lattice vector.[7]

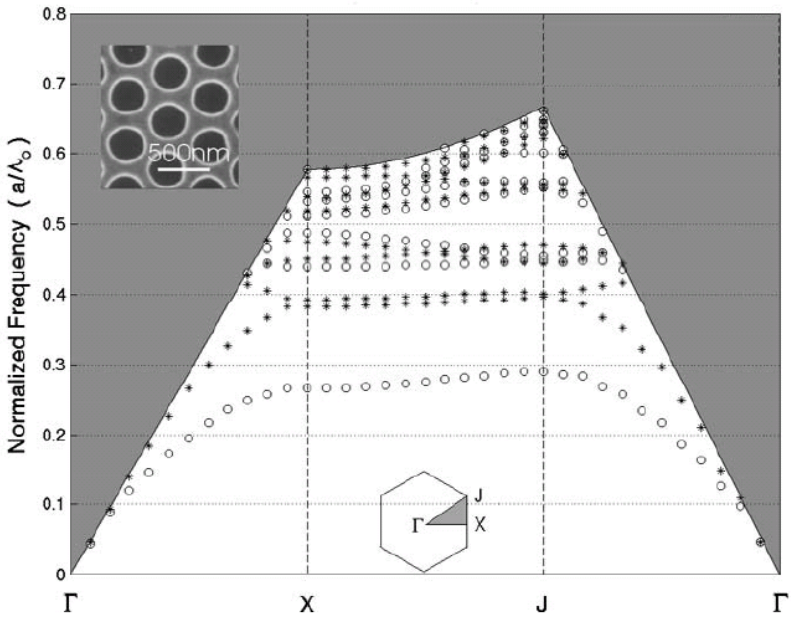

Figure 6: Band diagram of eigen modes of Si slab with 2D triangular lattice structure in the slab. The grey region represents the light cone where radiative modes reside. TE-like modes are illustrated by circles and TM-like ones are indicated by stars. Inset shows the SEM micrograph of the fabricated structure and its first Brillouin zone.[7]

Several parameters have influence on the properties of the 2D photonic crystal. The parameters include hole size, thickness of the slab and the refractive indices of both slab and

cladding materials. Using the same structure as the one used to calculate the band diagram, he finds that the photonic band gap becomes wider as the holes increase. Because the overlap with low-dielectric material (air) is enhanced, band edges are shifted towards higher frequencies when the hole size is enlarged. The influence of hole size is different for different types of modes. When holes are made too large (r/a > 0.5), the band gap for TE-like modes can be closed while that of TM-like modes can be opened. The band gap can also be closed when the holes are made too small. The slab thickness under investigation is in the range of approximately d/a = 0.3 – 0.7 so that single-mode condition is satisfied. However, changing the slab thickness does not have strong influence on the width of the band gap but the position of the band gap. Although today's design for 2D photonic crystal uses air as the cladding material, light can also be confined in the vertical direction if the cladding material has lower refractive index than that of the slab. Nevertheless, the light confinement becomes weak due to less contrast between refractive indices at the interface. Therefore, alternative cladding materials broaden the design space for a 2D photonic crystal microcavity.

2.2 Two-dimensional Photonic Crystal Laser Cavity

As previously discussed, no modes can propagate with frequencies inside the photonic band gap. However, by disrupting the lattice, we can induce a single mode or a set of modes within the gap. There are several ways of perturbing the lattice; for example, filling a hole in the lattice with a medium whose refractive index is different from other holes. In particular, if the filling material has the same refractive index as the slab, then this is equivalent to introducing a cavity in the lattice which is usually referred to the defect in photonic crystal. As a result, there may be a defect mode inside the cavity. This special mode must be evanescent meaning that it does not penetrate the rest of the crystal because the frequency is inside the band gap. If the cavity is properly designed such that it supports a mode in the gap, then light can be tightly confined around the defect. The intensity of the defect mode can be amplified through the interaction with gain media inside the cavity, generating a laser. The efficiency of the resonator is then measured as a value called the quality (Q) factor. Generally, the Q factor compares the frequency at which a system oscillates to the rate at which it dissipates its energy. In an optical system such as in the laser cavity, the Q factor of a resonant cavity is expressed as

$$Q = \frac{2\pi f_o \tilde{\varepsilon}}{P} \tag{2}$$

where f_o is the resonant frequency of the mode, $\tilde{\varepsilon}$ is the stored energy in the cavity and P is the dissipated power. Another important characteristic value is the mode volume which is defined as

$$V_{mode} = \frac{\int_V \varepsilon(r)|E|^2 dV}{\max\left[\varepsilon(r)|E|^2\right]} \tag{3}$$

where ε is the dielectric constant of the slab and E is the electric field amplitude of the mode. The integral is performed over the dimension of the field. We would like small mode volume to enhance the coupling of spontaneously emitted photons with the resonant mode. Therefore, a general design rule for a 2D photonic crystal laser cavity is to maximize the Q factor and obtain small mode volume at the same time. To illustrate the concept of a laser cavity design, a type of 2D photonic crystal cavity will be discussed as follows.

The L3 cavity design is proposed and optimized to suppress the loss in vertical direction. The structure of this type of cavity is shown in figure 7.[11] A two-dimensional photonic crystal slab perforated with air holes is the based structure. Then, three holes at the center of the slab are removed to perturb the periodicity of the lattice, thus creating a cavity for a defect mode. However, to suppress the scattering, two holes at the edge are slightly shifted to the sides. The shifting distance of the edge holes affects the Q factor. With this design, the Q factor is measured to be 45,000 and the mode volume is $7.0 \times 10^{-14} cm^3$. We will incorporate this structure in our proposed design for the current-injection photonic crystal laser.

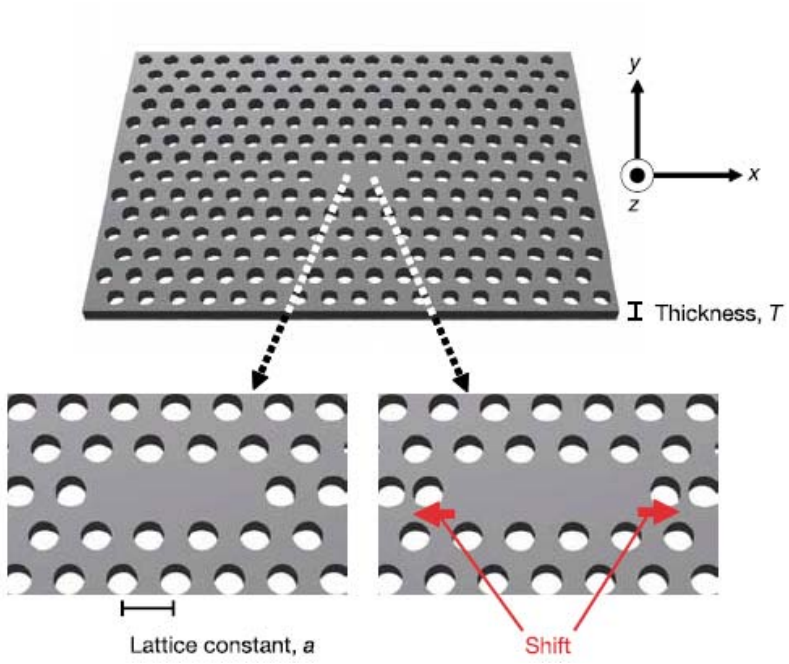

Figure 7: Optical nanocavities based on a 2D photonic crystal slab.[11]

Chapter 3: Design and Analysis of the Cladding Material

3.1 Current-Injection 2D Photonic Crystal Laser Design

We propose a design for a current-injection 2D photonic crystal laser as shown in figure below.

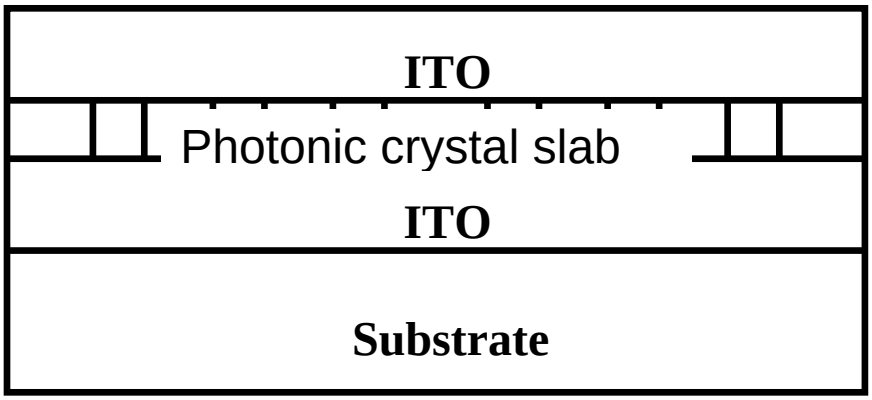

Figure 8: Structure of the current-injection 2D photonic crystal laser

Here, the photonic crystal is patterned on a semiconductor active material with quantum dots/wells embedded in it. The photonic crystal layer, which will be referred to as the membrane, is then sandwiched between the ITO layers. The entire structure is supported by a thick substrate. This design is simple and may not be efficient when performing measurement of the laser as will be discussed later in the fabrication process. The difference between this design and the conventional one is the cladding medium. We have incorporated a metal, Indium Tin Oxide or ITO, in our design as the electrodes allowing currents to reach the membrane with a pn junction, excite stimulated emission, and generate laser. The reasons for this choice of metal will be explained later. In our design, we implement the triangular lattice in our photonic crystal. We choose the L3-cavity design as discussed in the background.

3.2 Properties of ITO

ITO has unique optical properties. First of all, this type of metal is transparent and conductive. Its conductivity varies with deposition conditions. The ITO film must have high density of charge carriers for it to be conductive. However, the more charge carriers, the lower the transparency. A micron-thick ITO is typically yellowish to grey depending on its degree of oxidation. It is normally deposited by electron beam evaporation or sputtering techniques.

Apart from its physical properties, ITO also has attractive optical properties that, we believe, can be integrated with the photonic crystal laser. Various optical properties of SnO_2:F, which is another type conductors and similar to ITO, is studied.[12] For our design and analysis, we would like to know the refractive index spectrum of the cladding material. However, the refractive index of ITO varies with deposition parameters and thus it is difficult to pinpoint the exact values. Therefore, we refer to the results from the study of SnO_2:F for the approximate values of the refractive index of ITO. The spectra of real and imaginary parts of the refractive index of SnO_2:F are depicted in figure 9.

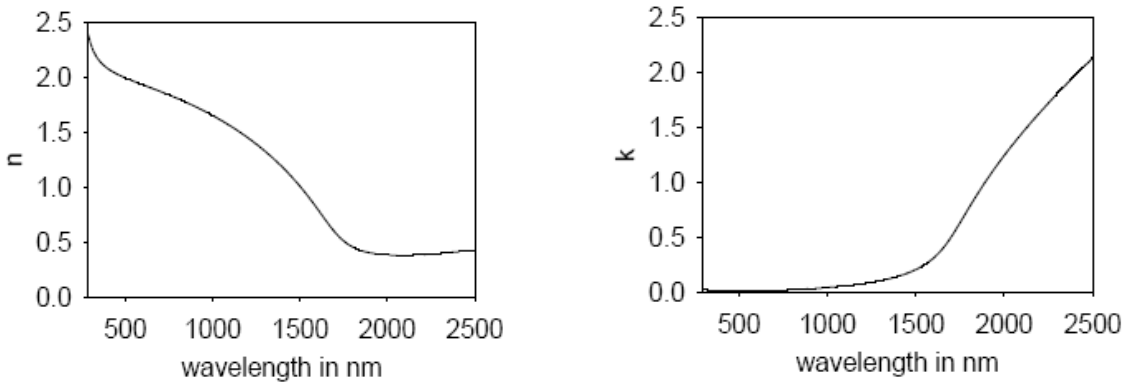

Figure 9: (Left) real and (Right) imaginary parts of the refractive index of SnO_2:F.[12]

From these spectra, the real part of the refractive index (n) is small comparing to the typical value of the refractive index of the semiconductor material used for photonic crystal slab e.g. 3.4 for our design. This makes ITO an appealing cladding material for the current-injection photonic crystal laser. Moreover, the extinction coefficient is not very high in the range of interest which is less than 1500 nm. The imaginary part of the refractive index signifies the loss mechanism created by the material. Therefore, low value of this coefficient is desired. For these reasons, we believe that ITO cladding photonic crystal should be able to obtain lasing. Finally, the fact that ITO varies with deposition conditions provides us more space when designing the structure of our laser.

3.3 Analysis of ITO refractive index

As the first step of laser cavity design, we analyze the refractive index of ITO based on our own fabricated samples. We use the radiofrequency (RF) sputtering technique to deposit ITO films on glass slides, varying deposition time. This will also vary thickness of the ITO on glass slides.

All the samples are grown at 12 mTorr of argon pressure and forward RF power of 175 W. Once the deposition is done, the thickness is measured using Scanning Electron Microscope (SEM). We made six samples and their thicknesses are listed in table 1.

Sample	Thickness (nm)	Deposition Time (min)
1	75	15
2	184	30
3	293	60
4	512	120
5	1200	240
6	2400	480

Table 1: Samples of ITO on glass slides

Then, we measure the transmittance of these samples over the wavelength interval of 500-1700 nm, using the spectrophotometer. The results of measurements are shown in table 2.

Wavelength (nm)	T1 (%)	T2 (%)	T3 (%)	T4 (%)	T5 (%)	T6 (%)
500	77.20	78.28	66.15	52.37	39.80	12.87
600	79.52	87.20	80.17	64.99	59.74	31.01
700	81.79	85.78	82.79	79.97	64.85	43.55
800	83.52	82.55	78.03	75.13	69.06	47.98
900	85.20	80.91	79.31	77.61	72.79	49.59
1000	86.77	80.61	83.17	81.95	64.56	42.46
1100	87.76	80.70	84.72	78.27	63.48	32.93
1200	88.37	80.85	83.62	72.68	53.89	21.54
1300	88.86	81.10	80.89	68.30	47.51	11.03
1400	88.94	80.67	76.93	64.11	38.94	5.10
1500	88.85	80.26	73.12	59.77	30.00	2.63
1600	88.50	79.33	69.16	55.15	22.45	1.53
1700	88.57	79.12	65.27	50.46	16.42	0.92

Table 2: Transmittance measurements of the ITO-glass samples

To obtain the theoretical model for the transmittance, we applied the optical analysis of thin films with the incoherent light source for the system as illustrated in figure 10. The ITO-glass layers are suspended in air. The refractive index of the glass is 1.43 and that of the air is 1. We assume that the only absorptive layer is ITO with complex refractive index denoted by $n_2 = n + ik$, where n represents its real part and k its extinction coefficient. The thickness of ITO is signified as d. Since the measurement setup of the spectrophotometer is such that the light is shone perpendicular to the surface of the sample, we assume normal incidence for the system. When the incoming light is incident on the air-ITO interface, it will be partially reflected and partially transmitted into the ITO layer. The ratios of the amplitudes of the reflected and transmitted beams to the corresponding incident beam can be described by the Fresnel's equations. For normal incidence, the amplitude reflection coefficient is defined as

$$r_{ij} = \frac{n_j - n_i}{n_j + n_i} \tag{4}$$

where i, j are the numbers corresponding to the first and the second layer, respectively, that light propagates through. Similarly, the amplitude transmission coefficient is written as

$$t_{ij} = \frac{2n_i}{n_j + n_i} \tag{5}$$

However, the analysis will involve light intensities rather than the field amplitudes because the interference effect is not strong in the system with incoherent light source. Consequently, we would like to express the ratio of the reflected and transmitted beams to the incident beam as the intensity coefficients which are defined as

$$R_{ij} = r_{ij} r_{ij}^{*} = \left(\frac{n_j - n_i}{n_j + n_i} \right)^2 \tag{6}$$

for the reflection and the intensity transmission coefficient can be written as

$$T_{ij} = \frac{n_j}{n_i} t_{ij} t_{ij}^{*} = \frac{4 n_i n_j}{\left(n_j + n_i \right)^2} \tag{7}$$

Light traveling through this layer will be attenuated due to the absorptive property of the ITO layer. The light intensity traveling through the layer for a distance x is described by Lambert-Beer law,

$$I(x) = I_o e^{-\alpha x} \tag{8}$$

where α is the absorption coefficient which is related to the imaginary part of the refractive index as

$$\alpha = \frac{4 \pi k}{\lambda} \tag{9}$$

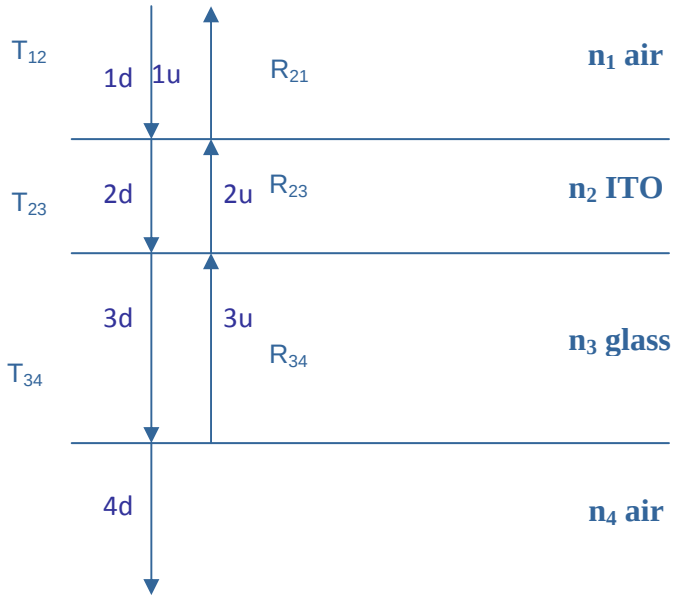

Figure 10: The two-layer system for the ITO refractive index analysis

The transmittance T of the sample is defined as the ratio of the reflected intensity I_t to the incident intensity I_o. Based on the diagram in figure 10, we can describe the propagation of light as shown in figure 11. The expression for transmitted light intensity is

$$I_t = T_{12} T_{23} T_{34} e^{-\alpha d} \sum_{l=0}^{\infty} \left(R_{34} R_{32} \right)^l \sum_{n=0}^{\infty} \left(R_{23} R_{21} e^{-2\alpha d} \right)^n \sum_{m=o}^{\infty} \left(T_{23} T_{32} R_{34} R_{21} e^{-2\alpha d} \right)^m I_o \tag{10}$$

The infinite series can be rewritten as

$$\sum_{n=0}^{\infty} x^n = \frac{1}{1-x} \tag{11}$$

for $|x| \ll 1$. Hence, the above expression, and $T = I_t / I_o$, can be simplified to

$$T = T_{12}T_{23}T_{34}e^{-\alpha d}\left(\frac{1}{1-R_{34}R_{32}}\right)\left(\frac{1}{1-R_{23}R_{21}e^{-2\alpha d}}\right)\left(\frac{1}{1-T_{23}T_{32}R_{34}R_{21}e^{-2\alpha d}}\right) \quad (12)$$

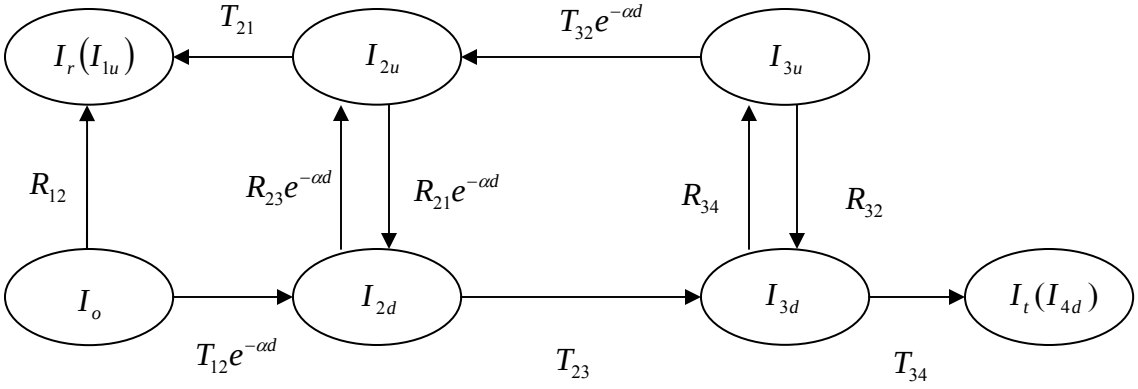

Figure 11: Diagram representing light propagation and the electric field amplitudes at various states in the ITO-glass system

Equation (12) represents the theoretical calculation of the transmittance which will be used to analyze the refractive index of ITO.

Next, we use equation (12) to calculate the transmittance corresponding to each set of data. In our approximation, we use the combination of two data sets from two samples to estimate the n and k values. By plotting the transmittance of the two data sets for each wavelength and find the intersection of the two transmittance values on the n-k plot, we can obtain the approximated values of n and k. For example, consider the combination of sample 1 with thickness of 293 nm and sample 2 with thickness of 2400 nm. Using MATLAB, we obtain the plot below.

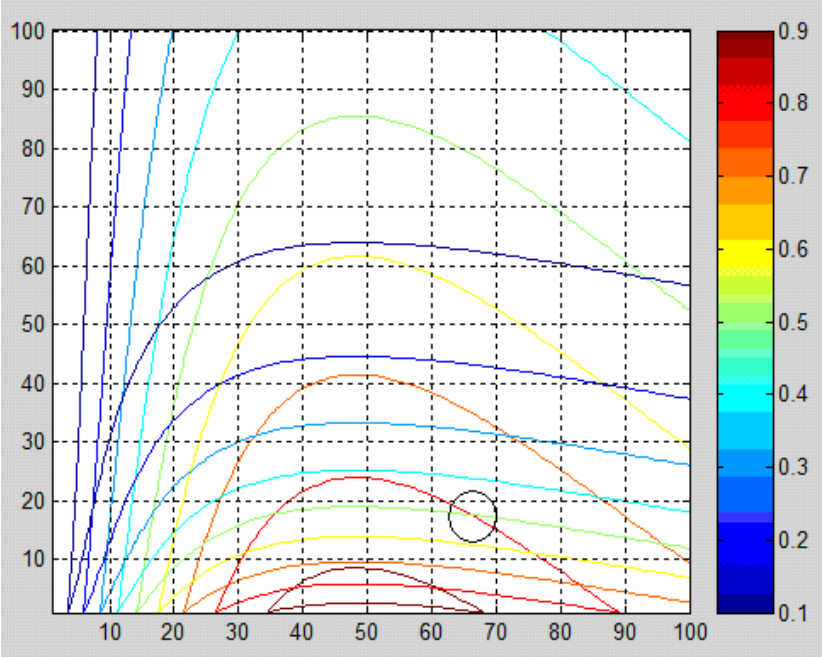

Figure 12: Superposition of the transmittance as a function of the ITO refractive index for thickness d1=293 nm and d2=2400 nm. The real part (n) and imaginary part (k) are on the y and x axes, respectively. Black circle shows the intersection used to determine the refractive index of ITO.

For this particular example, we specified the values of n from 0 to 2.3 and those of k from 0 to 0.05. The transmittance measured at the wavelength of 900 nm is 79.31% for sample 1 and 49.59% for sample 2. The black circle in figure 12 shows the intersection of the two transmittance values. The values of real and imaginary parts of the refractive index can be calculated from the coordinates of this point of intersection. Thus, from this particular example, the refractive index of ITO at 900 nm wavelength is 1.825+0.026i. By repeating the procedures, we obtained the refractive index spectra as illustrated in figure 13.

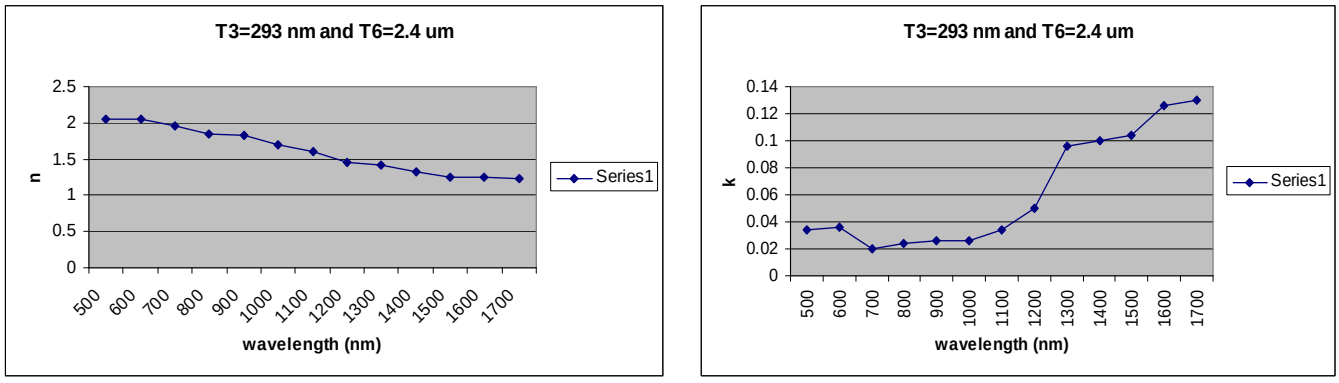

Figure 13: (a) real and (b) imaginary parts of the ITO refractive index as the result from the analysis.

Chapter 4: Implementation and Result

4.1 Band Diagram of ITO

Once we know the refractive index of ITO, we can now investigate our structure to find the potential for realizing a microcavity laser. At first, we calculate the band diagram of the photonic crystal sandwiched by ITO films. The band diagram shows the dispersion relation as a function of the propagation constant. To be able to design a structure for making a laser, we need to design a mode inside the photonic band gap for the ITO-clad photonic crystal slab structure. The photonic band gap allows us to design a cavity which will trap light and acts like a mirror for the mode to be localized inside the cavity. For this computational modeling, we employ the MIT Photonic-Bands (MPB) program which is based on plane-wave expansion method. The program is used to compute the photonic bands for periodic dielectric structure. This frequency-domain Maxwell's equation solver gives the mode frequencies at the given wave vector.

Triangular-lattice photonic crystal is analyzed. The hole radius is r = 0.3a, where a is the lattice constant. The slab thickness is d = 0.9a. The refractive index of the slab is 3.4 and that of ITO is set to 2.0, according to the analysis from the last section. We varied the index of the cladding ITO material, but the maximum value of ITO index used in the analysis is 2.0. Large index contrast provides a large photonic band gap, which is desirable for high-Q microcavity. Therefore, it is a challenge to design a high-performance microcavity with this setting. Photonic band gap is at least needed in this structure, so that we can design a microcavity based on this unique photonic crystal slab structure. In addition, holes are filled with silica because of the difficulty in fabrication as will be discussed later. The refractive index of SiO_2 is assumed to be 1.43. Figure 14 shows the result of band diagram calculation for the transverse electric (TE) like modes. The light blue line is the light line. We are only interested in the guided modes, which are under the light line, and these are represented by the pink and blue lines. The gap between these two lines defines the photonic band gap. The gap width is approximately 0.034. This calculation can be further optimized to enlarge the band gap and thus increasing the design space for the microlaser.

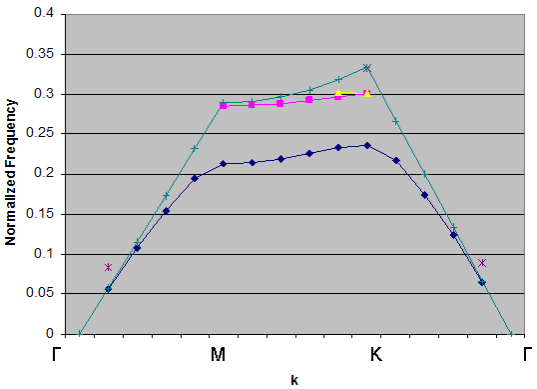

Figure 14: Band diagram calculation of TE modes in the proposed design

4.2 Microcavity

To determine the performance, we simulate the microcavity design and vary parameters, for optimization, which include the hole radius (r), the thickness of the membrane (d), the shifting

distance of the two holes at the edge of the cavity (d_shift), and the refractive index of ITO. The FDTD method is used to determine the Q factor of our microcavity design. In this technique, the computational space is divided into a discrete grid and then the fields are evolved in time using discrete time steps. As the grid and the time steps are made finer, the approximation becomes closer to the continuous equations. Some important results in this microcavity analysis are resonant frequency ω, the decay lifetime or the quality factor Q. The field profiles can be visualized. Periodic and/or absorbing boundaries are applied to the walls of the computational space. Then we excite the mode with a short Gaussian pulse from a current source placed inside the cavity. After the source is turned off, light propagation and field decay are analyzed.

We simulated the microcavity based on the same structure that we used in the band diagram analysis. The shifting distance of the edge holes is 0.2a. For telecommunication application, the target wavelength is 1.55 μm which corresponds to the ITO refractive index of 1.375+0.096i, according to our analysis. We use a temporal-Gaussian pulse with non-zero H_z component and it is placed slightly off-centered inside the cavity. Figure 15 shows field profiles of a TE mode that is confined inside the cavity. It is noted that negligible field is found outside the cavity in all directions. This mode has the normalized resonant frequency of 0.248 with the unit of 2πc/a, where c is the speed of light and a is the lattice constant as previously defined. The mode has the Q factor of 262 and the mode volume of 0.851 $(\lambda/n)^3$. Although the Q factor is much smaller than the value from the design shown in figure 7, we still believe that there is a good chance to obtain lasing operation using our microcavity designs because the minimum value of Q factor for potential lasing is about 100. However, we can further optimize the Q factor by modifying the design parameters or even changing the cavity design. Nevertheless, we would like to fabricate the current structure to test our hypothesis and see if we could obtain lasing operation.

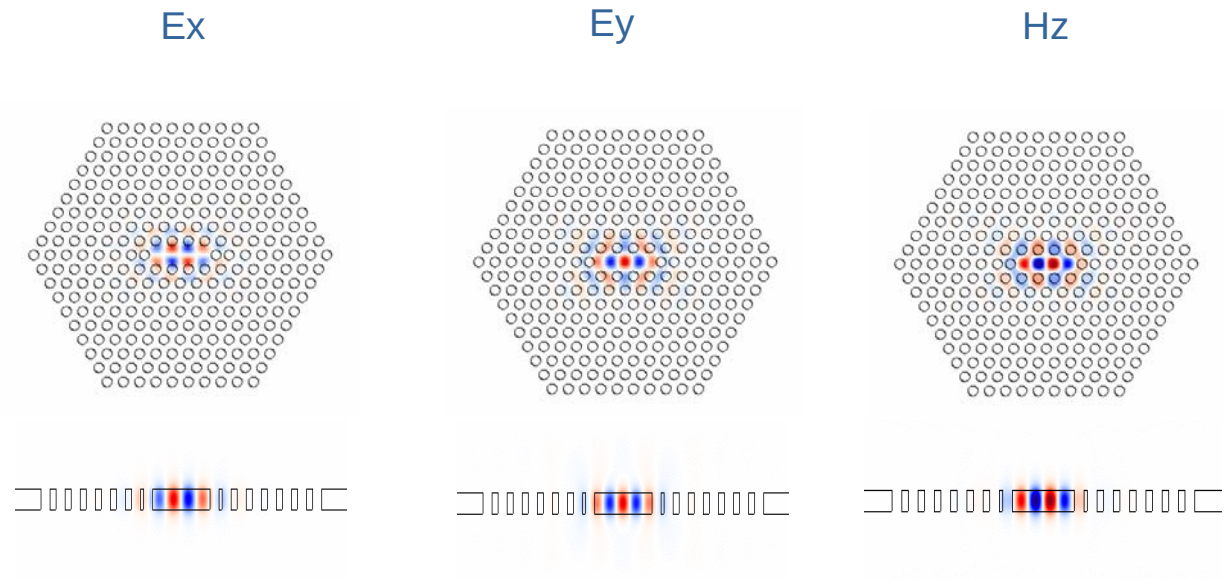

Figure 15: Cavity simulation of the proposed design.

4.3 Fabrication

We have fabricated our first sample based on the proposed design with a graduate student. However, according to the limited availability of the wafers, we use the AlGaAs/GaAs wafer with InGaAs quantum dots embedded in it. The quantum dots in the wafer have the emission wavelength of 1.3 μm. We also perform the simulation for the proposed design with the new index profile. In the simulation, all the settings are maintained but the refractive index of ITO is now changed to 1.675+0.056i at the emission wavelength of 1.3 μm. We find a mode with the resonant frequency of 0.246 in a unit of $2\pi c/a$. The Q factor is 220 and the mode volume is 0.888 $(\lambda/n)^3$. Since the result is not much different from what we obtained in the design with emission wavelength of 1.55 μm, we should be able to observe lasing for this microcavity structure.

There are many factors that we need to be considered in the fabrication process. Our proposed structure for fabrication is shown in figure 8. However, this structure needs to be modified to suit the measurements. An array of microcavity devices are fabricated on one chip. These devices needed to be separated for electrical isolation. Thus, we modify the structure from figure 8 to the new one as in figure 16. The fabrication techniques required for fabricating this structure include ITO deposition, epitaxial lift-off, wafer bonding, SiO_2 coating, and lithography. In the following section, we would like to discuss the ITO deposition, the epitaxial lift-off method and the Van der Waals bonding, since I am particularly involved in these processes.

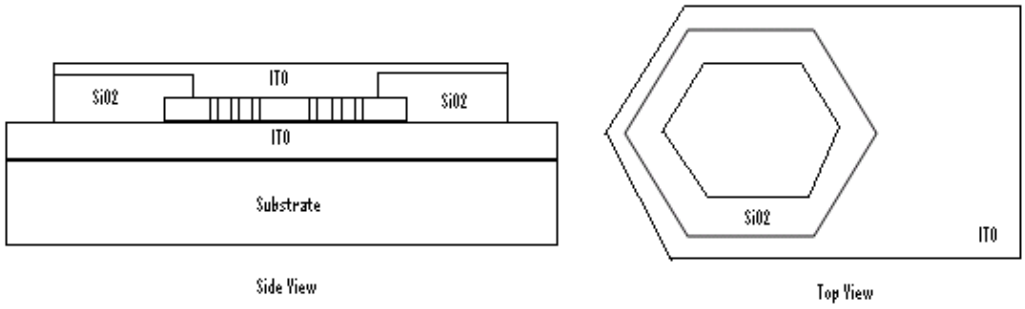

Figure 16: Modified structure for the proposed design to separate the devices for testing

4.3.1 ITO deposition

We choose the radio-frequency (RF) sputtering technique to deposit ITO films on a substrate. The Kurt Lesker PVD 75 RF dielectric sputter system is used for this purpose. The substrate is placed on the round plate which rotates when deposition is in process. The deposition condition is set to 12 mTorr of argon pressure and forward RF power of 175 W at room temperature. We set the deposition time to two hours and obtain the ITO thickness of approximately 600 nm.

4.3.2 Epitaxial Lift-Off

In order to obtain thin-film, active III-V semiconductor slabs, we use the epitaxial lift-off technique. The wafer structure of our wafer is shown in figure 17. We want to use the InGaAs/GaAs QD active regions for our laser. We refer to the method developed in [1 and 9]. First, the wafer is cleaned in acetone to remove any organic contaminants. Then, we deposit the diluted black wax (Apiezon W) in dichloromethane (DCM) (25 g wax: 100 ml DCM) on top of

the wafer. The wafer with the black wax is then annealed at 120 degree C for 30 minutes and air cured for another 30 minutes. The black wax plays an important role in the epitaxial lift-off process. It essentially creates tension to lift up the corners of the epitaxial film which includes the GaAs cap, the GaAs active layers embedded in the 16.5% AlGaAs layers, thus enhancing the channel for diffusion in the etching process. After the film of black wax is formed, the wafer is left overnight in the buffered-oxide etchant (BoE) 6:1. The BoE solution will etch away the 94% AlGaAs sacrificial layer. Finally, we obtain the thin film containing the active region separated from the thick substrate as desired.

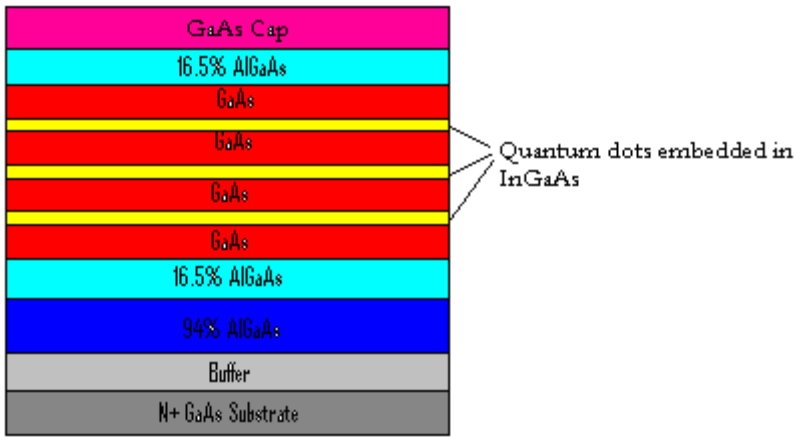

Figure 17: Layer structure of the AlGaAs/GaAs wafer used to fabricate the photonic crystal slab in the proposed design

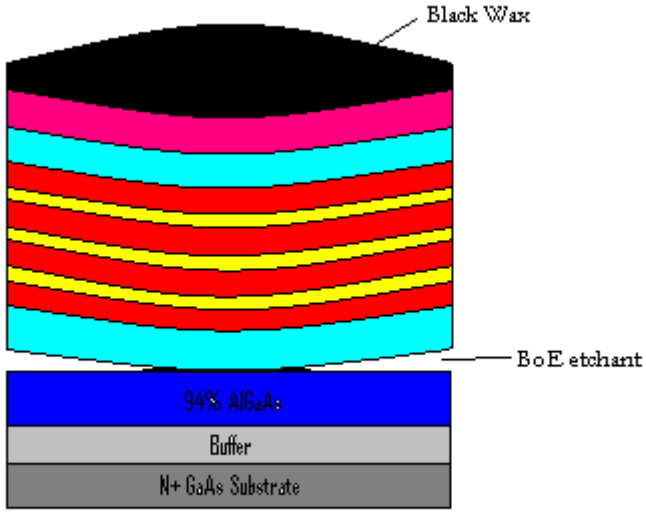

Figure 18: Black wax is coated on the wafer, creating tension to lift the corners of the wafer and enhancing the channel for diffusion of the BoE etchant

4.3.3 Van der Waals bonding

After the epitaxial lift-off process, the thin film is bonded with the ITO layer on a substrate. We refer to a technique called Van der Waals bonding in [1 and 10]. The separated wax-coated thin film is placed onto the ITO layer on the substrate. This process takes place under deionized (DI) water. The surface tension of the DI water initially pulls the film down to the ITO-substrate layer. Then, pressure must be applied so that the remaining water is absorbed in the lens paper. The setup and process are illustrated in figure 19. In our case, after successfully transferring the wax-coated film to the ITO-substrate layer using a vacuum pen, we leave the entire structure under a weight of approximately 20 g/mm^2 for one night. After bonding, we remove the wax by dissolving it in the DCM. Finally, the sample is ready for the lithography of the photonic crystal pattern.

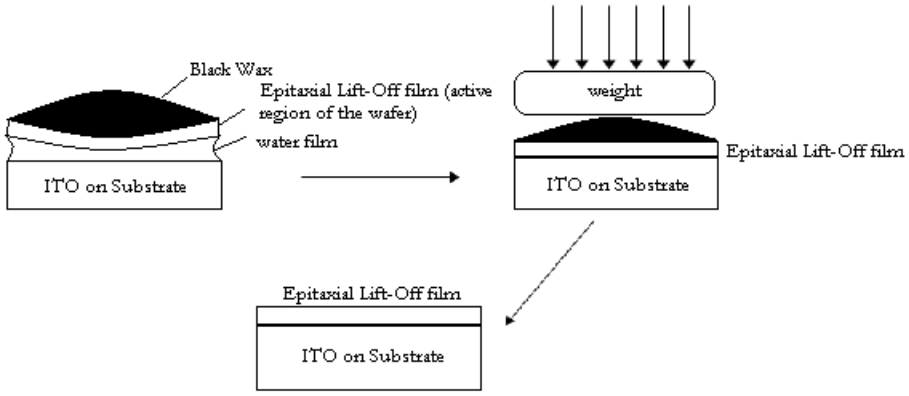

Figure 19: The Van der Waals bonding procedure

4.4 Measurement

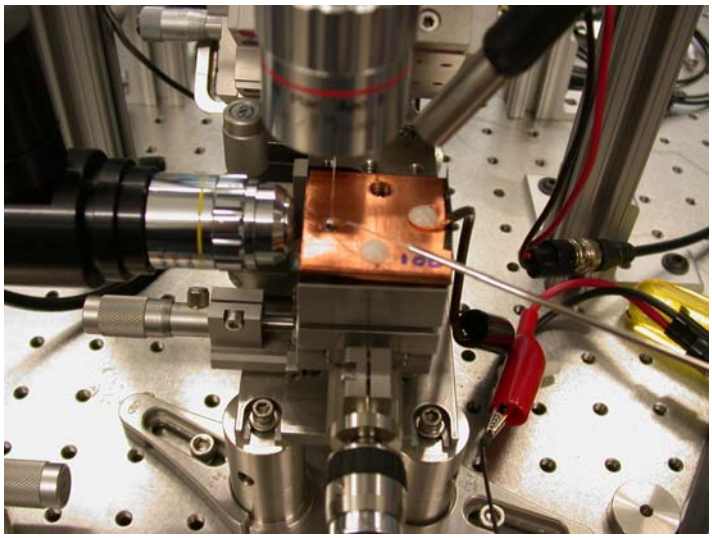

Figure 20: Measurement setup for collecting output light emission and sending it to an optical spectrum analyzer

We have set up the test station to measure the light emission from the fabricated sample as in figure 20. The sample is bonded on the conducting plate or the copper plate in this case which is connected to the negative lead of the voltage source. A narrow-width electrical probe is placed on the top electrode of the sample for electrical pumping. The optical fiber is used to collect light from the sample and send the output to the spectrum analyzer. The spectrum analyzer will then give the electroluminescence spectrum of the emission from the sample. We have fabricated and tested one chip and, currently, we are optimizing the fabrication processes to improve the electrical properties of the current-injection photonic crystal microcavities.

Chapter 5: Conclusion

The fabricated sample did not show diode-like voltage-current characteristics. One factor that inhibits the lasing operation in our sample comes from imperfections in fabrication process. For example, the bonding strength is not sufficient, resulting in discontinuity of the surfaces between the layers. If this was the case, there will be another air layer between the photonic crystal slab and ITO layers. Each electrode contact should be ohmic, and we are investigating the electrical properties of ITO/GaAs junctions.

For higher chance of lasing operation, we will optimize the design to obtain higher Q factor with small mode volume. There are many design parameters that we can explore to achieve this goal; for example, the refractive indices of ITO, the hole radius, the slab thickness, the shifting distance of the two cavity-edge holes, and the cavity design.

In conclusion, we have proposed a new design for the current-injection two-dimensional photonic crystal slab microcavity. Simulations suggest the possibility to achieve lasing operation in this structure. We have fabricated one sample and tested it; however, we did not observe the lasing operation. We are currently investigating the fabrication techniques and optimizing the design for higher Q.

References

1. Demeester, P. et al. “Epitaxial Lift-Off and Its Applications.” Semiconductor Science and Technology 8 (1993): 1124-1135.
2. Hecht, Eugene. Optics (4th Edition). Addison Wesley, 2001.
3. Jacob, W. et al. “Infrared Analysis of Thin Films: Amorphous, Hydrogenated Carbon on Silicon.” Brazilian Journal of Physics. vol. 30, no.3 (2000).
4. Joannopoulos, J. D. et al. Photonic Crystals: Molding the Flow of Light. Princeton: Princeton University Press, 1995.
5. Johnson, Steven. Meep-AbInitio. April 10, 2009. <http://abinitio.mit.edu/wiki/index.php/Meep>.
6. Johnson, Steven. MIT Photonic Bands. April 10, 2009. <http://ab-initio.mit.edu/wiki/index.php/MPB>.
7. Loncar, Marko. “Nanophotonic Devices Based on Planar Photonic Crystals.” PhD thesis California Institute of Technology, 2003.
8. Park, H. G. et al. “Electrically Driven Single-Cell Photonic Crystal Laser.” Science 305 (2004): 1444.
9. Yablonovitch, E. et al. “Extreme Selectivity in the Lift-Off of Epitaxial GaAs Films.” Applied Physics Letters 51 (1987): 2222.
10. Yablonovitch, E. et al. “Van der Waals Bonding of GaAs on Pd Leads to a Permanent, Solid-Phase-Topotaxial, Metallurgical Bond.” Applied Physics Letters 59 (1991): 3159.
11. Akahane Y. et al. “High-Q Photonic Nanocavity in a Two-dimensional Photonic Crystal.” Nature 425 (2003): 944-947.
12. Rottkay, von K. et al. “Optical Indices of Pyrolytic Tin-Oxide Glass.” Material Research Society Symposium Proceedings 426 (1996): 449.